Chinese Journal of Chemical Engineering 28 (2020) 1964–1972

Contents lists available at ScienceDirect

Chinese Journal of Chemical Engineering

journal homepage: www.elsevier.com/locate/CJChE

Article

Adsorption equilibrium and the effect of honeycomb heat exchanging device on charge/discharge characteristic of methane on MIL-101(Cr) and activated carbon

Guobin Zhao, Qingrong Zheng *, Xuan Zhang, Weidong Zhang

Provincial Key Laboratory of Naval Architecture & Ocean Engineering, Institute of Marine Engineering, Jimei University, Xiamen 361021, China

ARTICLE INFO

Article history:
Received 21 February 2020
Received in revised form 24 April 2020
Accepted 30 April 2020
Available online 17 May 2020

Keywords:
Natural gas
MOFs
Activated carbon
Adsorption

ABSTRACT

Experiments were conducted for developing suitable ANG adsorbents for vehicular applications. MIL-101 and activated carbon samples were respectively prepared by hydrothermal and chemical activation methods. Two samples were undergone structure analysis on adsorption data of nitrogen at 77.15 K, and adsorption data of methane were then volumetrically measured within temperature–pressure range 293.15 K–313.15 K and 0–8 MPa. A conformable vessel in volume 2.5 L was employed for charge/discharge tests under the flow rate 10–30 L·min^{-1}. It shows that limit isostreic heat of methane adsorption is respectively about 25.15 kJ·mol^{-1} and 22.94 kJ·mol^{-1} on the activated carbon and the MIL-101, and isosteric heat within the experimental condition is 14–19.5 kJ·mol^{-1}; employing a smaller charge/discharge flow rate can weaken the temperature fluctuation of the adsorbent bed and increase the charge/discharge amount; employing honeycomb heat exchanging device enhance the thermal conductivity of the adsorbent bed by consuming a negligible part of volume of the vessel. It suggests that a smaller flow rate for charge/discharge should be employed, and MOFs together with the honeycomb heat exchanging device are promising for practical applications.

1. Introduction

ANG, which can bring about a comparable storage density of methane to that of CNG under a lower pressure, has been being regarded as one of the most promising approaches for onboard storage of natural gas since 1980s [1,2]. However, gaps between the targets recently set by the U.S. Department of Energy (DOE) and results from researches are considerable, lacking of high performance adsorbents is still a bottleneck in developing ANG technique.

Early in 1980s, carbon based materials were considered to be the most suitable adsorbents for storage of natural gas because of their much lower costs and light weights [3–5]. However, numerous studies have so far shown that carbon based adsorbents having high microporosities and surface areas larger than those of the ideal graphene can only obtain the storage density of methane about 160V/V [6], which is less than the target 180V/V and 263V/V respectively set by the DOE in 2000 and 2012 [6,7], let alone 350V/V recently set for commercialization of ANG [8]. Since Kondo reported experimental result of methane adsorption on a kind of three-dimensional framework in 1997, due to its unique advantage of extensive structural diversity and tenability, researching interests have also been increasingly aroused on metal–organic frameworks (MOFs) which have been considered to be promising adsorbents for methane storage [9]. Large amount of researches have been conducted experimentally and theoretically to analyze the relations between the adsorptive performance and the effects from the structures, ligands, functionalities, open metal sites, framework density, surface area and pore volume [10]. Analyses of adsorption equilibrium, which are also crucial to ANG, have also been performed to determine the adsorption model for accurately predicting the adsorption data and the isosteric heat of adsorption for obtaining useful information about the interaction between the adsorbate and the adsorbent [11–13]. From the relevant research [6], it shows that, dissimilar to those of natural gas storage by adsorption on carbon based materials where a larger specific surface area and microporous volume are always beneficial to enhancing their storage capacities, MOFs has an optimal specific surface area and microporous volume suitable for practical applications of ANG, and the packing density as well as structural stability of MOFs should also be typically emphasized while taking into account of its gravimetric and volumetric storage capacities of methane at 298 K and 3.5 MPa [14–19]. Moreover, management of the thermal effects resulted from the heat from adsorption and compression of the adsorbate is vital to the application of ANG. In general, thermal effect can be weakened by heat transfer enhancement on the storage system by taking such measures as inserting a heat exchanger, adding the expanded natural graphite (ENG) or phase change materials into the adsorbent

* Corresponding author.
E-mail address: qrzheng816@sina.com (Q. Zheng).

https://doi.org/10.1016/j.cjche.2020.04.021

bed [20–22], but these measures sacrifice part of the volume of the vessel and possibly decrease the storage amount. Meanwhile, application of ANG calls for the densification of the adsorbent pellets or powders and the structural optimization of the storage tank, matching among the measures mentioned above is therefore a necessity for improving the storage density of the system [23,24]. Additionally, prolonging the duration of charge and discharge processes was also suggested by some researchers, but these may be unreasonable since the rate of charge or discharge should be in conformity with the requirement for practical needs [16].

To obtain useful information for developing ANG adsorbents, this paper directly compares the adsorptive performance of methane on currently focused adsorbents on two aspects. MIL-101 and the activated carbon are the selected adsorbents synthesized in the laboratory, analysis of adsorption equilibrium of methane on two samples is one aspect which was performed based on the structural characterization, adsorption data of methane measured in very low pressure range and a high pressure range in correspondence with the temperatures required by ANG. Dynamic characteristic of methane on the adsorbent bed of the two samples was evaluated by employing a conformable vessel under typical charge and discharge rates of methane. The effect of inserting a honeycomb heat exchanging device on mitigating the thermal effect was also evaluated.

2. Experimental

2.1. Materials

The MIL-101 sample was prepared by hydrothermal method in soft conditions without hydrofluoric acid. Chemical activation was employed to synthesize the activated carbon, chitosan was selected as carbon source, and KOH was as activating agent; more information about the synthesis has been described in elsewhere [25–27].

Thinking about that the adsorbed phase of methane in its supercritical state can sometimes be considered as a quasi-liquid, and both nitrogen and methane are nonpolar molecules whose diameters are respectively about 0.364 nm and 0.39 nm, it is reasonable to analyze the adsorption equilibrium of methane as per the structural parameters determined by adsorption data of nitrogen at 77.15 K. Here, structural characterizations of the prepared samples were conducted on the adsorption data of nitrogen at 77.15 K measured by employing Micromeritics 3Flex, and pore size distributions (PSDs) and specific surface areas of the samples were respectively determined *via* non-local density functional theory (NDFT) calculation and the BET plot.

2.2. Measurements of adsorption isotherms

Adsorption isotherms of methane on as-prepared MIL-101 and activated carbon samples were measured within a temperature range in correspondence with that required by ANG. Two kinds of automated Sieverts apparatus, which are Micromeritics 3Flex and Setaram PCTPro E&E, were employed to measure the adsorption equilibrium data respectively under a very low pressure range and a higher pressure range. In comparing 0.0607 g MIL-101 and 0.0360 g activated carbon samples used while employing Micromeritics 3Flex, about 0.4313 g MIL-101 and 0.6063 g activated carbon samples were undergone tests on Setaram PCTPro E&E. Activated carbon filters were placed at the exit of gas source to wipe off the water vapor in gas. The used gases (methane, nitrogen and helium) are of ultra-high-purity grade and they were from Air Liquide Xiamen Co Ltd.

Prior to each adsorption test, the sample was placed in vacuum at 423.15 K for 24 h to expel any residual gas from it. It was in the state of de-gassing in two apparatuses at 423.15 K for 3 h after the sample has been loaded. The temperature of the reference cell was maintained at 303.15 K with a stability of 0.01 K. The temperature of the adsorption cell for Setaram PCTPro E&E and the adsorption tube for Micromeritics 3Flex was accurately maintained and controlled with circulating coolant supplied by a Julabo with a stability of 0.01 K. To ensure the accuracy of the experimental data, the test was repeated four times and the mean value of the equilibrium data was used to calculate the adsorption isotherm, more information about the experiment can be found in elsewhere [28,29].

2.3. Charge/discharge tests

For fully comparing adsorptive performance and evaluating the effect of heat management measures on methane adsorption on two samples, charge and discharge tests were specially designed. As those shown in Fig. 1, natural gas discharged from a storage tank is led to a fuel supply pipe for a marine diesel engine whose type is C4190Z_{LC}-2.

A storage vessel, which is schematically shown in Fig. 2, is a conformable type whose capacity is enough to supply sufficient fuel for the engine running under its typical load condition about 10 min. Schematically shown in Fig. 3 is an aluminum alloy honeycomb heat exchanging device used for heat transfer enhancement of the adsorbent bed. For comparing, charge and discharge tests were conducted on the vessel respectively packing with two adsorbent samples; the effect of the heat exchanging device was also evaluated. Thinking about that the fuel consumption rate of the engine is about 10 L·min^{-1}–30 L·min^{-1} at typical working conditions, charging of the vessel was

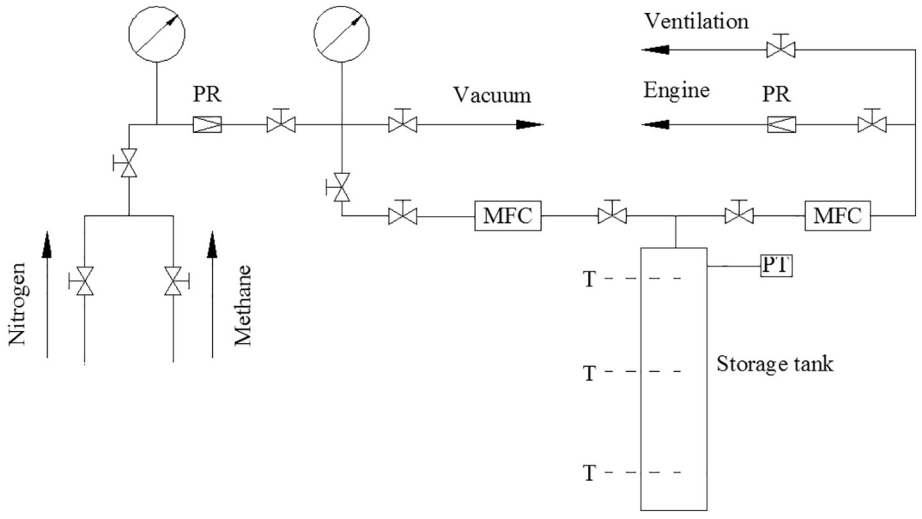

Fig. 1. Schematic diagram of the test rig for charge and discharge of fuel gases.

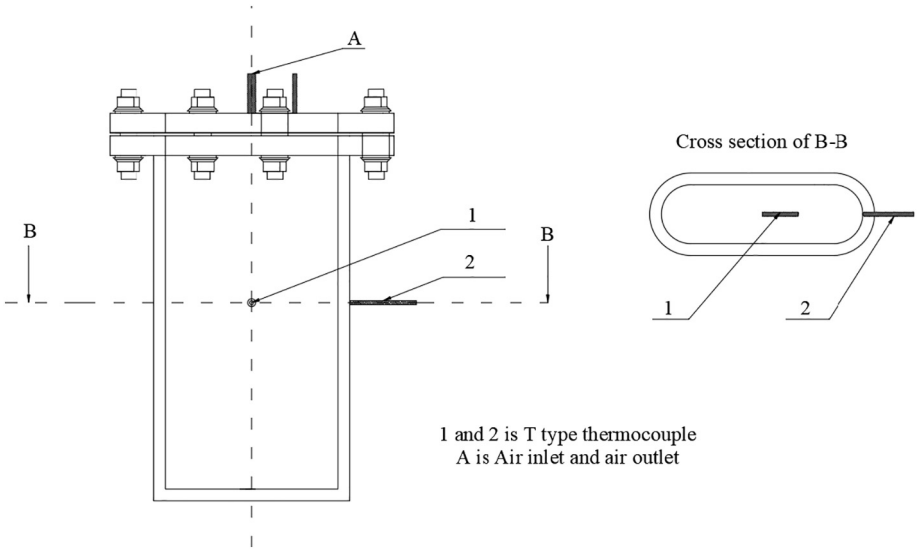

Fig. 2. Schematic diagram of the structure of a conformable tank.

performed by methane at pressure 3.5 MPa under the flow rate 10 L·min^{-1}–30 L·min^{-1} accurately set by mass flow controller (MFC), and discharging of the vessel began just after the charge tests under the similar flow rate.

Table 1 shows the main parameters related with the tests. During the tests, the temperature and relative humidity of the laboratory was maintain at 20 °C and 65 ± 5% by running air conditioners; temperatures at the central region of the adsorbent bed and the wall of the vessel were recorded, pressure within the vessel and the flow rate of charge and discharge were also measured for evaluating the factors influencing the thermal effect [23,30]. Here, mean values of the experimental results, which resulted from charge and discharge tests repeatedly performed four times, were used to improve their accuracies.

Table 1
Main parameters for charge and discharge tests

Adsorbents	Honeycomb heat exchanging device	Amount of the adsorbent/g	Packing density of the adsorbent/g·ml^{-1}
MIL-101	Without	950	0.38
	With	930	0.37
Activated carbon	Without	980	0.45
	With	950	0.41

3. Results and Discussions

3.1. Structural characterization of the samples

As those shown in Fig. 4a, isotherms on both samples are type I, it suggests that only monolayer adsorption of nitrogen occurred on two samples. It can be observed in Fig. 4b that, within micro-pore region, in comparing with one peak in PSD of the activated carbon, the PSD of MIL-101 sample has two peaks locating around pore width about 0.7 nm and 0.9 nm.

As noted in Table 2, both samples are rich in micro-pores and have a similar mean pore width, MIL-101 has a larger specific surface area but a much smaller ratio of surface area within micro-pore region. Thinking about that the kinetic diameter of a methane molecule is about 0.38 nm, it suggests that both synthesized samples should have good adsorptive performances for methane molecules in supercritical region but may have different adsorption behaviors due to the differences in structures.

3.2. Adsorption equilibrium

As those shown in Figs. 5 and 6, in very low pressure range, adsorption amounts on both adsorbents almost linearly increase with the increase of the equilibrium pressure and the relation between them can be described by Henry law; while the equilibrium pressure gets higher, both isotherms exhibit the characteristic of excess amount of physical adsorption of supercritical gases, isotherms gradually reach their maximums at certain pressures [31,32].

An obvious characteristic can be found by comparing adsorption isotherms shown in Figs. 5 and 6, which notes that, at very low pressure region, adsorption amount on MIL-101 is smaller in comparing with that of the activated carbon, but the situation is reverse while the pressure gets higher where adsorption amount on the MIL-101

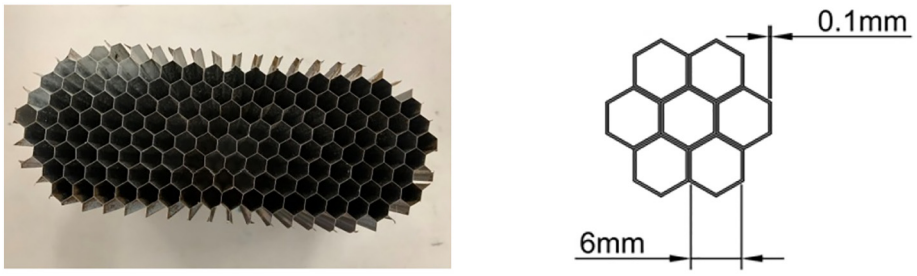

Fig. 3. Schematic diagram of the honeycomb heat exchanging device.

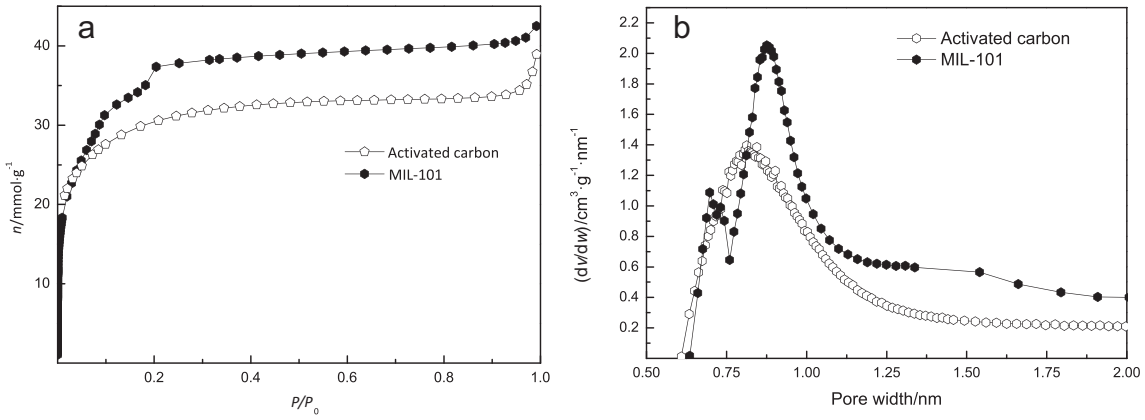

Fig. 4. Isotherm (a) of nitrogen at 77.15 K and the PSD (b) of both samples.

Table 2
Structural parameters of the MIL-101 and activated carbon

Sample	BET specific surface area/$m^2 \cdot g^{-1}$	Mean pore width/nm	Micro-pore volume/$cm^3 \cdot g^{-1}$	Ratio between specific surface area from micropores and that of the sample/%
MIL-101	3164	1.86	1.09	18.27%
Activated carbon	2229	1.83	1.23	62.88%

is much larger than that on the activated carbon. These can be ascribed to the different behavior of methane adsorption on these two kinds of adsorbents, as mentioned in relevant researches [33], in very low pressure region, adsorption capacity of supercritical gas is closely related with the value of the surface area contributed by micropores; while equilibrium pressure gets higher, the main determinant factor to the adsorption amount is the value of the specific surface area.

In very low pressure region, the variation between adsorption amount and equilibrium pressure will be.

$$n = H_p \cdot P \tag{1}$$

Here, H_P is the Henry law's constant; P is the equilibrium pressure. The limit isosteric heat of adsorption q_{st0} and H_P has the relationship as

$$q_{st0} = RT + R\left(\frac{\mathrm{d}\ln H_p}{\mathrm{d}\frac{1}{T}}\right) \tag{2}$$

where R is the gas constant; T is the equilibrium temperature. H_P determined by the plot of adsorption data shown in Figs. 5a and 6a and q_{st0} calculated by Eq.(2) are listed in Table 3.

Adsorption amounts volumetrically measured are the excess adsorption amounts, which need to be converted into absolute adsorption amounts for engineering purposes.

As per Gibbs's definition of the adsorption [32], the excess adsorption amount n_{exc} can be correlated with absolute adsorption amount n_{abs} as

$$n_{exc} = n_{abs} - v_a \cdot \rho_g = v_a\rho_a - \rho_g = n_{abs}\left(1 - \frac{\rho_g}{\rho_a}\right) \tag{3}$$

Where v_a is the specific volume of adsorbed phase; ρ_g the density of bulk gas phase; ρ_a the density of adsorbed phase. Here, ρ_g is also determined by the EOS presented by Setzmann and Wagner [34].

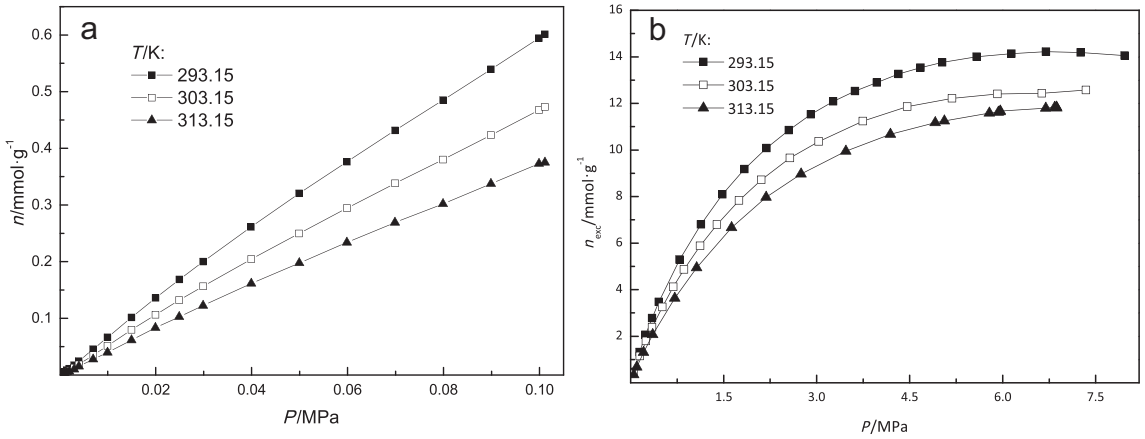

Fig. 5. Isotherms of methane adsorption on MIL-101 at low pressure ranges (a) and high pressure ranges (b).

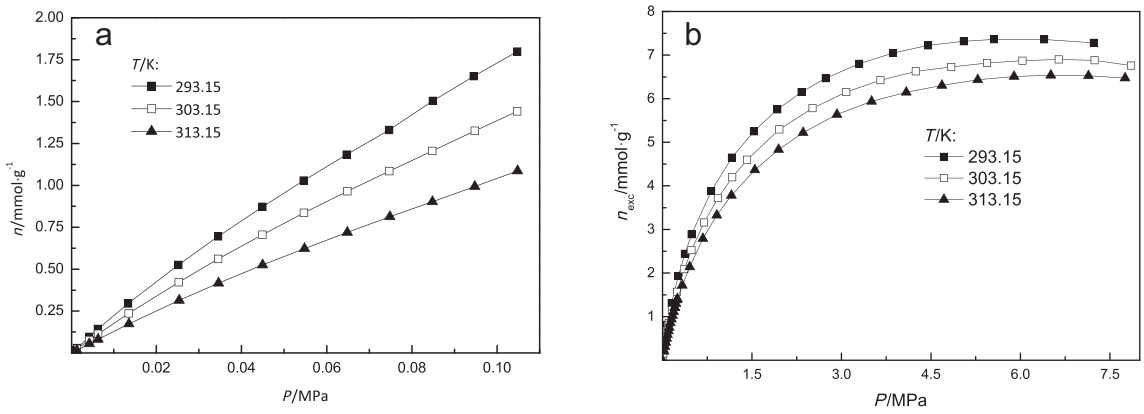

Fig. 6. Isotherms of methane adsorption on activated carbon at low pressure ranges(a) and high pressure ranges(b).

Table 3
Thermodynamic parameters of methane adsorption on two samples at very low pressure range

Sample	T/K	H_P/mmol·Pa^{-1}·g^{-1}	q_{st0}/kJ·mol^{-1}	Mean limit isosteric heat of adsorption/kJ·mol^{-1}
Activated carbon	293.15	2.12×10^{-5}	25.06	25.15
	303.15	1.67×10^{-5}	25.15	
	313.15	1.12×10^{-5}	25.23	
MIL-101	293.15	3.77×10^{-6}	22.86	22.94
	303.15	3.07×10^{-6}	22.94	
	313.15	2.21×10^{-6}	23.02	

From previous studies [35,36], it can be observed that n_{exc} can be accurately described by Toth equation, that's

$$n_{exc} = n_0 \frac{(bf)^t}{\left[1+(bf)^t\right]^{1/t}}\left(1-\frac{\rho_g}{\rho_a}\right) \tag{4}$$

Here n_0 is the saturation adsorption capacity;f is the bulk gas fugacity; b and t parameters which can be nonlinearly determined by fitting the experimental data *via* Eq. (3).

The mean deviation δ is used to evaluate the accuracy of fitting, that's

$$\delta = \frac{1}{N}\sum_{i=1}^{N}\frac{|n^i_{exc}-n^i_{cal}|}{n^i_{exc}}\times 100\%, \tag{5}$$

Here N is the equilibrium points of one isotherm; n^i_{exc} experimental excess adsorption amount at ith equilibrium point; n^i_{cal} the excess adsorption amount predicted by Toth equation.

The results were shown in Table 4 and Fig. 7. The δ on MIL-101 and activated carbon samples was respectively 1.06% and 0.24%, which verifies the accuracy of the fitting equations.

Isosteric heat of adsorption n can be calculated by the Clausius–Clapeyron (C–C) equation [36], that's

$$q_{st} = -R\left[\frac{\mathrm{d}\ln f}{\mathrm{d}(1/T)}\right]_n \tag{6}$$

where R is the universal gas constant; f the fugacity in correspondence with the equilibrium pressure; T the temperature; n the adsorption amount. Here, the equation of state (EOS) presented by Setzmann and Wagner is used to determine the fugacity.

Adsorption isosteres from absolute amounts determined by Toth equation were plotted on by using Eq. (6), results are shown in Fig. 8. From Fig. 8, it notes that, within the experimental conditions, isosteric heats on two samples are almost within the same range 14–19.5 kJ·mol^{-1}.

3.3. Charge and discharge tests

3.3.1. Charge tests

Charging of the vessel was performed at the flow rate 10 L·min^{-1} and 30 L·min^{-1}, temperature fluctuations recorded at the central region and the wall of the vessel are shown in Fig. 9. As shown in Fig. 9, the temperature fluctuation on both the central region and the wall had been mitigated by using a smaller flow rate of charge, and storage system suffered from a stronger thermal effect while the vessel was packed with MIL-101. These phenomena backup the argument that a smaller flow rate of charge should be employed where the slow charge is permitted, otherwise measures for heat transfer enhancement should be taken to weaken temperature fluctuation of the adsorbent bed.

In 'b' frame of Fig. 9, the scale of temperature variation at the wall of the vessel packed with the activated carbon is larger than that packed with the MIL-101, which can be interpreted as a smaller thermal conductivity of the synthesized MIL-101 sample in comparing with that of the activated carbon sample, measures for heat transfer enhancement on the adsorbent bed of MIL-101 are therefore more necessary since the sample has a larger capacity for methane adsorption than the activated carbon.

Table 4
Parameters of Toth equation determined by nonlinearly fitting of experimental data

Temperature/K	Adsorbent	δ	n_0/mol·g^{-1}	b/MPa^{-1}	t	v_a/cm^3·g^{-1}
293.15	MIL-101	1.08%	0.05066	0.2294	0.6613	1.4218
	Activated carbon	0.28%	0.02595	0.6152	0.4867	0. 8771
303.15	MIL-101	1.20%	0.03017	0.2839	0.8855	1.2946
	Activated carbon	0.44%	0.02119	0.5591	0.5425	0.7372
313.15	MIL-101	0.91%	0.04204	0.2102	0.6792	1.5188
	Activated carbon	0.31%	0.01656	0.5368	0.6208	0.5269

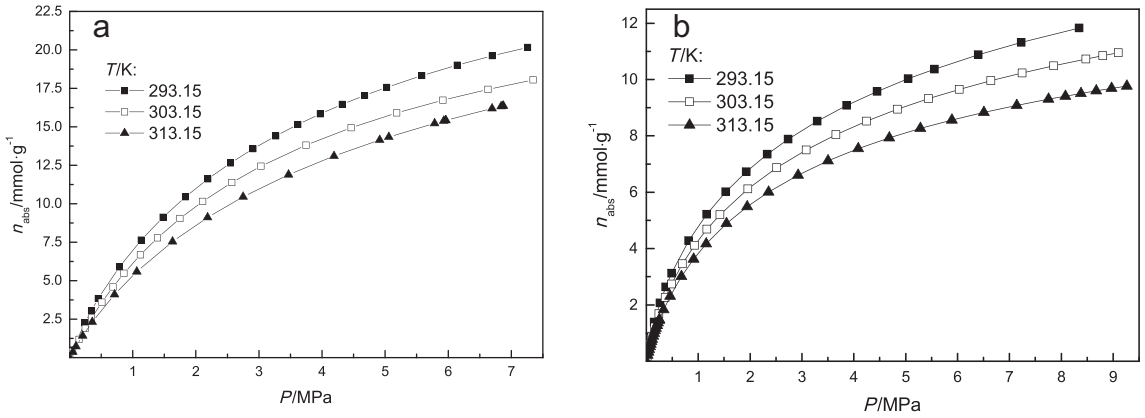

Fig. 7. Isotherms of absolute amount of methane adsorption on MIL-101 (a) and activated carbon (b).

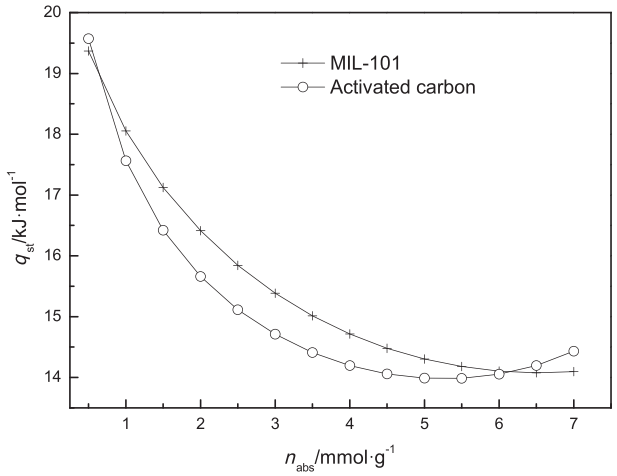

Fig. 8. Isosteric heat of methane adsorption on MIL-101 and activated carbon determined by Clausius–Clapeyron equation.

The accumulated amount of in-charged methane within the storage vessel is shown in Fig. 10. Table 5 shows the main parameters summarized from the data measured during the charging processes under two flow rates, it notes that a smaller flow rate of charge is beneficial to lowering down the temperature of the adsorbent bed and increasing the charged amount within a certain charge duration, which suggests that the flow rate can be as small as possible where the duration for charging is long enough. Meanwhile, the comparison among the results in Fig. 10 and Table 5 also reveals that the accumulated amount of the charge is closely related with the adsorption capacity of the adsorbent, due to a larger specific surface area and micropore volume, the accumulated amount of methane contained within the storage vessel packed with MIL-101 is almost twice while packing with the activated carbon sample. Moreover, an obvious characteristic can be found in Fig. 10, under the same flow rate, for the storage vessel packed with MIL-101, the duration for the accumulated charge amount reaches its maximum (here, the duration is defined as effective charge duration T_e) is much longer than that where the activated carbon is used, T_e is about 1930 s and 590 s in comparing with 1090 s and 320 s respectively in corresponding with the flow rate of charge 10 L·min^{-1} and 30 L·min^{-1}. Thinking about that the slow charge isn't always permitted, measures for shortening T_c should therefore be taken.

3.3.2. Discharge tests

Discharging of the storage vessel was conducted directly after the charge tests at the corresponding flow rates, temperature records and the accumulated amount of discharge were respectively shown in Figs. 11 and 12. As noted in Fig. 11, similar to the results in previous studies [29], temperature fluctuation on both adsorbent beds gets stronger while a larger flow rate is employed, these also suggest the necessity of equipping heat recovery measures since the discharge flow rate should meet with the fuel consumption rate required by the engine. Similar to the records in charging process, adsorbent bed packed with MIL-101 suffered from a much severer temperature fluctuation than

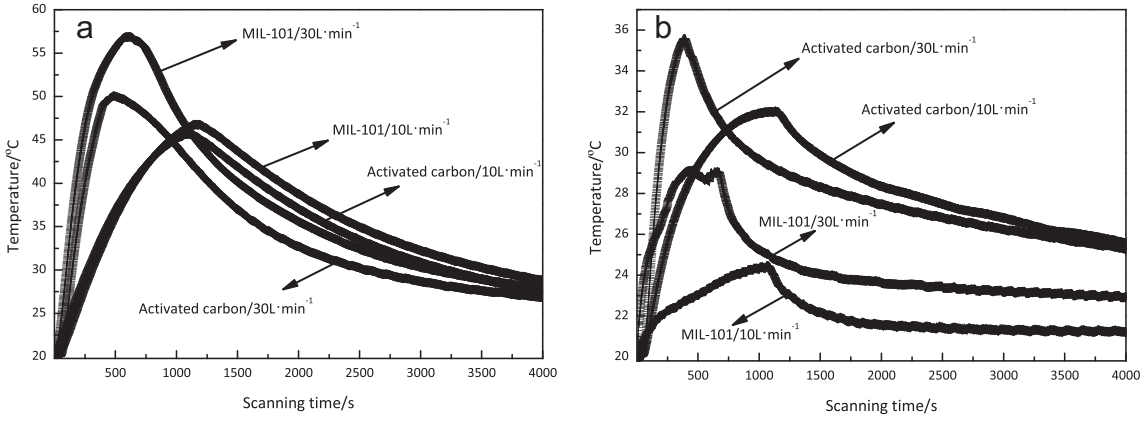

Fig. 9. Variations of temperature at the center (a) and the wall (b) of the storage vessel during the charge.

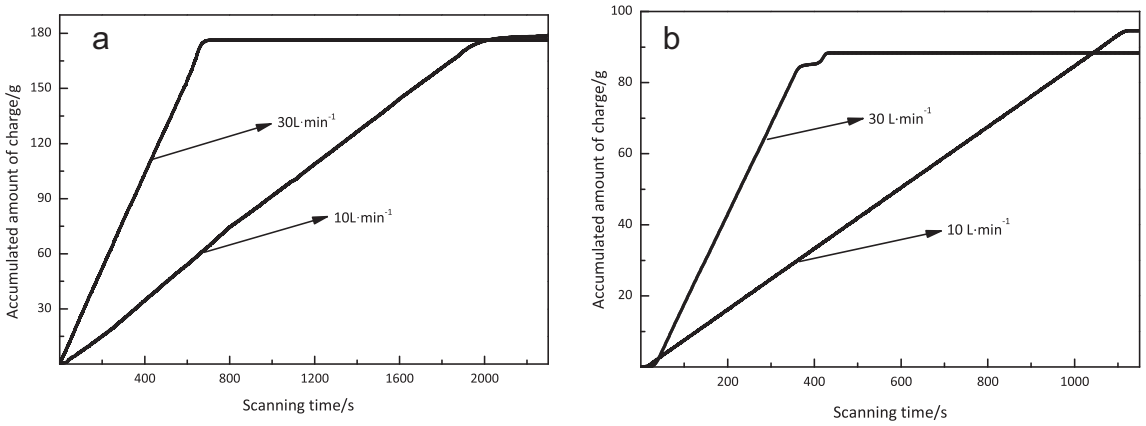

Fig. 10. The accumulated amount of charge on the vessel packed with MIL-101 (a) and activated carbon (b) at different flow rates.

Table 5
Related data on charging process

Adsorbent	Amount of charge/g		Mean temperature rise of the adsorbent bed/°C		Maximum rise of the temperature of the adsorbent bed/°C		Effective charge duration T_c/s	
	10 L·min^{-1}	30 L·min^{-1}	10 L·min^{-1}	30 L·min^{-1}	10 L·min^{-1}	30 L·min^{-1}	10 L·min^{-1}	30 L·min^{-1}
MIL-101	178.6	176.1	16	23	27	37	1930	590
Activated carbon	94.7	88	19	23	26	30	1090	320

that of the activated carbon, and the gap between them becomes larger where a larger flow rate is employed.

In Fig. 12, the influence of variation of the flow rate on the discharged amount of methane is obvious, a larger flow rate brought about a larger amount of discharged methane within a shorter period of time, but the increasing rate of accumulated amount of discharge under a smaller flow rate became larger than that under a larger flow rate within a longer period of time. Since a greater fluctuation of the temperature within a storage system will exert a stronger thermal stress on the storage vessel and accordingly bring about safety issue, it is therefore a need to select a reasonable rate for discharge *via* optimization by taking into account such factors as the fuel consumption rate required by the engine, structure of the vessel and the thermal stress of the vessel.

Results from further comparison of the data shown in Figs. 11 and 12 are listed in Table 6. As noted in Table 6, the effect of the temperature fluctuation of the adsorbent bed on the discharge amount is obvious, a smaller flow rate of discharge prolongs the effective charge duration T_d (the duration for the discharge amount reaches its maximum) but is beneficial to increasing the discharge amount. Meanwhile, Table 6 also reveals the fact that measures are needed to compensate the heat for weakening the temperature fluctuation especially on the storage system of the MIL-101 who has a relatively smaller thermal conductivity.

3.3.3. Effect of heat transfer enhancement

MIL-101 was selected for verification tests which were conducted under the flow rate 30 L·min^{-1}, results are shown in Fig. 13 and Table 7. From the data listed in Table 7, the effect of inserting a honeycomb heat exchanging device is significant, under the flow rate 30 L·min^{-1}, which brings about the drops of the maximum and mean temperature variation amplitudes of the storage system about 19 °C and 12 °C for charge, 24 °C and 22 °C for discharge, respectively.

By further comparing with the corresponding accumulated charge and discharge amount listed in Tables 5 and 6, it can be found that, by inserting a honeycomb heat exchanging device, accumulated amount

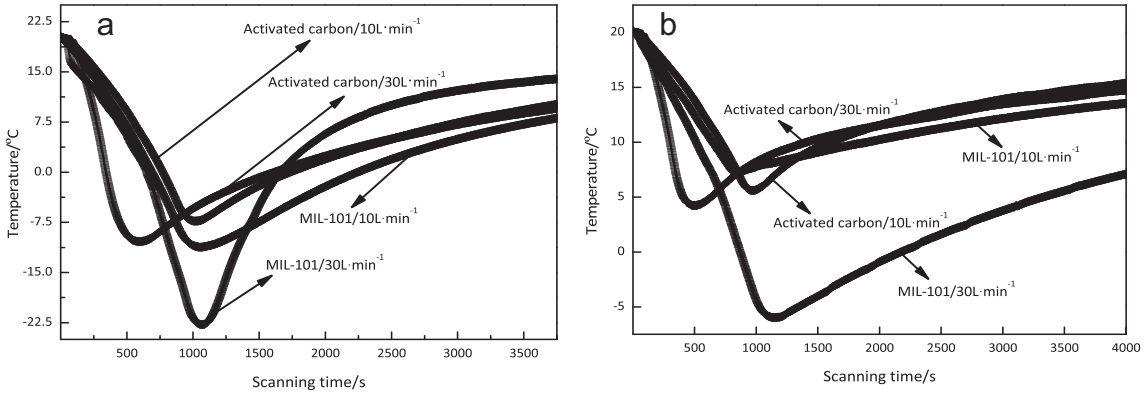

Fig. 11. Temperature records at the center (a) and the wall (b) of the vessel during the discharge.

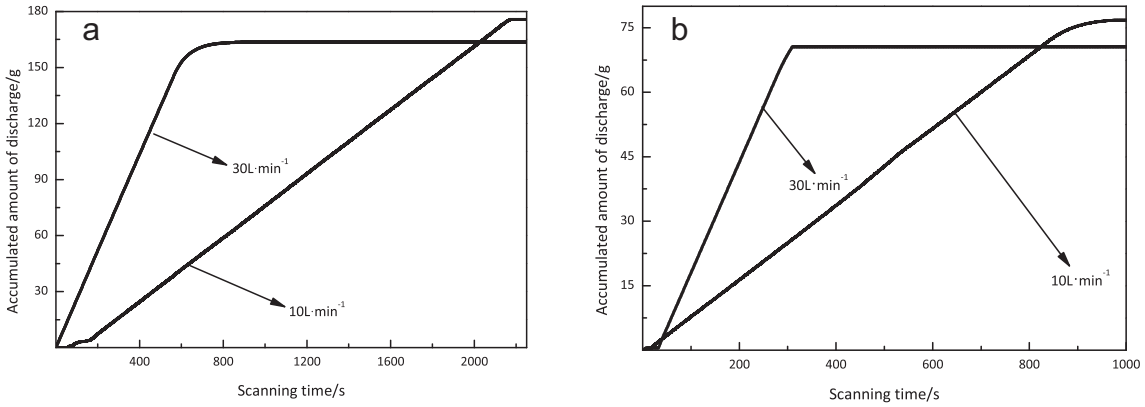

Fig. 12. The accumulated amount of discharge from the vessel packed with MIL-101 (a) and activated carbon (b) at different flow rates.

Table 6
Related data from discharging process

Adsorbent	Amount of discharge/g		Mean drop of temperature of the adsorbent bed/°C		Maximum drop of the temperature of the adsorbent bed/°C		Effective discharge duration T_d/s	
	10 L·min^{-1}	30 L·min^{-1}	10 L·min^{-1}	30 L·min^{-1}	10 L·min^{-1}	30 L·min^{-1}	10 L·min^{-1}	30 L·min^{-1}
MIL-101	175.5	163.7	22	34	32	45	2090	710
Activated carbon	76.7	70.5	21	23	28	30	840	260

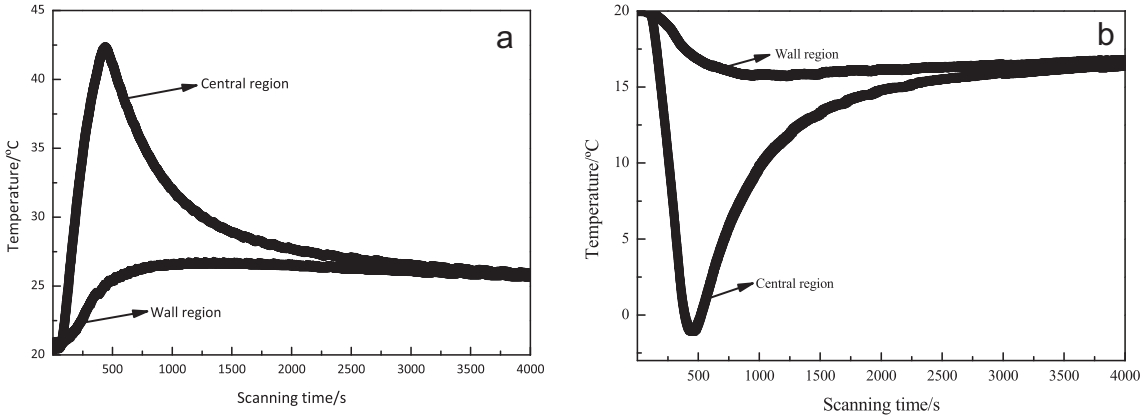

Fig. 13. Temperature variation at the storage vessel during charging (a) and discharging (b) processes with equipping heat exchanging device.

of charge decreases from 176.1 g to 174 g, but the discharge amount increases from 163.7 g to 169.3 g. It suggests that equipping a honeycomb heat exchanging device is an efficient approach to managing the thermal effect on ANG storage system.

4. Conclusions

Aimed at developing an efficient storage medium for ANG, and based on the adsorption equilibrium of methane on the activated carbon and MIL-101, dynamic characteristics of an ANG vessel respectively packed with two adsorbents at different flow rates, effect of inserting a honeycomb heat exchanging device within the adsorbent bed, the conclusions can be summarized as follows:

1. The behavior of methane adsorption on MIL-101 and activated carbon samples is different due to the difference in their structures. Within the temperature range 293.15 K–313.15 K, the limit isosteric heat of methane adsorption on MIL-101 and activated carbon is

Table 7
Related data of charging and discharging processes at flow rate 30 L·min^{-1}

Processes	Amount of charge or discharge/g	Mean value of temperature change at the adsorbent bed/°C	Maximum change of the temperature at the adsorbent bed/°C	Effect on mitigating the temperature fluctuation/°C	
				Mean value of temperature change at the adsorbent bed	Maximum change of the temperature of the adsorbent bed
Charge	174	11	16	12	19
Discharge	169.3	13	21	22	24

respectively about 22.94 kJ·mol^{-1} and 25.15 kJ·mol^{-1}, but isosteric heats at the same temperature region and under pressure range 0-8 MPa are almost the same. The MIL-101 sample has a specific surface area about 3164 m^2·g^{-1} but that contributed by micro-pores is about 633 m^2·g^{-1} in comparing with 1382 m^2·g^{-1} of the activated carbon, which leads to their different behaviors of methane adsorption at very low pressure range and high pressure range.

2. Thermal conductivity of the MIL-101 is smaller than that of the activated carbon, employing a smaller flow rate of charge or discharge is beneficial to cutting down the temperature fluctuation of the adsorbent bed and increasing charge/discharge amount within effective charge/discharge periods. In comparing with the flow rate 30 L·min^{-1}, for a conformable vessel in volume 2.5 L packed with MIL-101 and activated carbon respectively about 950 g and 980 g, the scale of variation of temperature had correspondingly 10 °C and 12 °C reduction respectively in charge and discharge processes, which further brought about 2.5 g and 11.8 g increment of the charge and discharge amounts.
3. Employing honeycomb heat exchanging device is an effective method for enhancing the thermal conductivity of the adsorbent bed by consuming a negligible part of the volume of the storage vessel. For the tested vessel, under the flow rate 30 L·min^{-1}, by inserting a honeycomb heat exchanging device, the maximum and mean temperature variation amplitudes of the storage system can have 19 °C and 12 °C drop for charge, 24 °C and 22 °C drop for discharge, respectively; accumulated amount of charge decreases from 176.1 g to 174 g, but the discharge amount increases from 163.7 g to 169.3 g.

Acknowledgements

The project was supported by National Natural Science Foundation of China (51979121).

References

[1] H.D. Zhang, P. Deria, *et al.*, A thermodynamic tank model for studying the effect of higher hydrocarbons on natural gas storage in metal-organic frameworks, *Energy Environ. Sci.* 8 (2015) 1501–1510.
[2] X.S. Chen, B. Mcenaney, T.J. Mays, *et al.*, Theoretical and experimental studies of methane adsorption on microporous carbons, *Carbon* 35 (1997) 1251–1258.
[3] J. Alcañiz-Monge, M.A.D.L. Casa-Lillo, D. Cazorla-Amorós, *et al.*, Methane storage in activated carbon fibres, *Carbon* 35 (1997) 291–297.
[4] M. Molina-Sabio, C. Almansa, F. Rodriguez-Reinoso, Phosphoric acid activated carbon discs for methane adsorption, *Carbon* 41 (2003) 2113–2119.
[5] J.P. Marco-Lozar, M. Kunowsky, F. Suárez-García, *et al.*, Activated carbon monoliths for gas storage at room temperature, *Energ Environ Sci* 5 (2012) 9833–9842.
[6] K.V. Kumar, K. Preuss, M.M. Titirici, *et al.*, Nanoporous materials for the onboard storage of natural gas, *Chem. Rev.* 117 (2017) 1796–1825.
[7] T. Burchell, M. Rogers, SAE Technical Paper Series [SAE International Government/Industry Meeting, (JUN. 19, 2000)] SAE technical paper series - low pressure storage of natural gas for vehicular applications, SAE Transactions Washington USA 109 (2000) 2242–2246.
[8] Methane Opportunities for Vehicular Energy, Advanced Research Project Agency – Energy, U.S. Dept. of Energy, Funding Opportunity no. DE-FOA-00006722012.
[9] M. Kondo, T. Yoshitomi, H. Matsuzaka, *et al.*, Three-dimensional framework with channeling cavities for small molecules:{[M_2(4,4′-bpy)$_3$(NO_3)$_4$]·xH_2O}$_n$(M = Co, Ni,Zn), *Angew Chem Int Edit* 36 (1997) 1725–1727.
[10] H. Xu, J. Chen, S.L. Luo, *et al.*, Relationship between activated carbons structure and its properties of methane gas adsorption, *Carbon Tech* 1 (2016) 15–19 (In Chinese).
[11] S. Ma, H.C. Zhou, A metal-organic framework with entatic metal centers exhibiting high gas-adsorption affinity, *J. Am. Chem. Soc.* 128 (2006) 11734–11735.
[12] T. Düren, L. Sarkisov, O.M. Yaghi, *et al.*, Design of new materials for methane storage, *Langmuir* 20 (2004) 2683–2689.
[13] C. Liang, Z. Shi, C.T. He, *et al.*, Engineering of pore geometry for ultrahigh capacity methane storage in mesoporous metal organic frameworks, *J Am Chem Soc* 139 (2017) 13300–13303.
[14] N. Bimbo, J.A. Physick, A. Noguera-Díaz, *et al.*, High volumetric and energy densities of methane stored in nanoporous materials at ambient temperatures and moderate pressures, *Chem. Eng. J.* 272 (2015) 38–47.
[15] X.S. Chen, B. Mcenaney, T.J. Mays, *et al.*, Theoretical and experimental studies of methane adsorption on microporous carbons, *Carbon* 35 (1997) 1251–1258.
[16] K.A. Rahman, W.S. Loh, A. Chakraborty, *et al.*, Thermal enhancement of charge and discharge cycles for adsorbed natural gas storage, *Appl. Therm. Eng.* 31 (2011) 1630–1639.
[17] K.J. Chang, O. Talu, Behavior and performance of adsorptive natural gas storage cylinders during discharge, *Appl. Therm. Eng.* 16 (1996) 359–374.
[18] L.L. Vasiliev, L.E. Kanonchik, D.A. Mishkinis, *et al.*, Adsorbed natural gas storage and transportation vessels, *Int. J. Therm. Sci.* 39 (2000) 1047–1055.
[19] M. Bastos-Neto, A.E.B. Torres, D.C.S. Azevedo, *et al.*, A theoretical and experimental study of charge and discharge cycles in a storage vessel for adsorbed natural gas, *Adsorption* 11 (2015) 147–157.
[20] L.L. Vasiliev, L.E. Kanonchik, D.A. Mishkinis, *et al.*, Adsorbed natural gas storage and transportation vessels, *Int. J. Therm. Sci.* 39 (2000) 1047–1055.
[21] S. Biloe, V. Goetz, S. Mauran, Dynamic discharge and performance of a new adsorbent for natural gas storage, *AIChE J.* 47 (2001) 2819–2830.
[22] C. Zhang, X.S. Lu, A.Z. Gu, The adsorption heat research status of natural gas and hydrogen adsorption storage, *Acta Energi Sin* 25 (2004) 249–253.
[23] Q.R. Zheng, Z.W. Zhu, Y.L. Feng, *et al.*, Development of composite adsorbents and storage vessels for domestically used adsorbed natural gas, *Appl. Therm. Eng.* 98 (2016) 778–785.
[24] Q.R. Zheng, Z.W. Zhu, X.H. Wang, Experimental studies of storage by adsorption of domestically used natural gas on activated carbon, *Appl. Therm. Eng.* 77 (2015) 134–141.
[25] C. Ferey, C. Mellot-Draznieks, C. Serre, *et al.*, A chromium terephthalate-based solid with unusually large pore volumes and surface area, *Science* 309 (2005) 2040–2042.
[26] L. Bromberg, Y. Diao, H.M. Wu, *et al.*, Chromium(III) terephthalate metal organic framework(MIL-101): HF-free synthesis. Structure, Polyoxometalate Composites, and Catalytic Properties, *Chem Mater* 24 (2012) 1664–1675.
[27] Khasri, Azduwin, Bello, *et al.*, Mesoporous activated carbon from Pentace species sawdust *via* microwave-induced KOH activation: Optimization and methylene blue adsorption, *Res Chem Intermediat* 44 (2018) 5737–5757.
[28] W.D. Zhang, Q.R. Zheng, Z.H. Wang, *et al.*, Adsorption equilibrium of methane on layered graphene sheets and activated carbon, *J. Fuel Chem. Technol.* 47 (2019) 1008–1015.
[29] G.B. Zhao, Q.R. Zheng, W.D. Zhang, *et al.*, Adsorption equilibrium and charge/discharge characteristics of methane on MIL-101, *J. Fuel Chem. Technol.* 47 (2019) 1529–1936.
[30] M.J. Prosniewski, T.A. Rash, E.W. Knight, *et al.*, Controlled charge and discharge of a 40L monolithic adsorbed natural gas tank, *Adsorpt* 24 (2018) 541–550.
[31] Y.P. Zhou, B. Yang, Progress in studies on supercritical adsorption of gases, *Chem Bull* (2000) 8–13 (In Chinese).
[32] P.G. Menon, Adsorption at high pressures, *Chem. Rev.* 68 (1968) 277–294.
[33] D.P. Cao, G.T. Gao, W.C. Wang, Grand canonical ensemble Monte Carlo simulation of adsorption storage of methane inslit micropores, *J Chem Ind Eng* 51 (2000) 24–29 (In Chinese).
[34] U. Setzmann, W. Wagner, A new equation of state and tables of thermodynamic properties for methane covering the range from the melting line to 625 K at pressures up to 100 MPa, *J. Phys. Chem. Ref. Data* 20 (1991) 1061–1155.
[35] N. Bimbo, W. Xu, J.E. Sharpe, V.P. Ting, *et al.*, High-pressure adsorptive storage of hydrogen in MIL-101 (Cr) and AX-21 for mobile applications: Cryocharging and cryokinetics, *Mater Design* 89 (2016) 1086–1094.
[36] S. Gao, Q.R. Zheng, Comparisons of adsorption models for methane adsorption equilibrium on activated carbon, *J. Fuel Chem. Technol.* 41 (2013) 380–384.